heavy clay soils and for the deeper soil horizons (the soil depth used by Post *et al.* was 1 m). The setting of clay content at 20% for all soils is another obvious source of error: if, for example, the clay content of the tropical forest wet zone is set at 10, 20 and 30%, the calculated inputs of carbon for equilibrium in this zone are 17.3, 15.3 and 14.4×10^{15} g C yr^{-1}, respectively.

The soil carbon estimates in Table 1 do not include surface litter: if this is included, the discrepancy between calculated input and global NPP will increase, although the effect is small. Consider the worst case, that of boreal forest. If, following Schlesinger[21], boreal forest contains 13% of its total soil organic carbon in surface litter, then the calculated annual input of carbon from the (combined) boreal forest moist and wet zones, allowing for surface litter, is 6.3×10^{15} g C yr^{-1}, not 5.5×10^{15} as in Table 1.

In the model the decomposability of the incoming plant material is set by the DPM/RPM ratio and errors will result if this ratio is incorrect. The value of 0.25 used in Table 1 for all the forests is taken from work on deciduous trees at Rothamsted (D.S.J., D. D. Harkness, E. D. Vance, D.E.A. and A. F. Harrison, manuscript in preparation) and may be too large for the more resistant debris from coniferous forest. If so, the calculated annual inputs of carbon given in Table 1 for the boreal forests are too big.

As the model gave plausible results on the world scale, we then used it to calculate how much CO_2 would be released from the world stock of soil organic carbon if world temperatures rose uniformly by 0.2, 0.3 or 0.5 °C per decade. These are the lower limit, best estimate and upper limit suggested by the IPCC report[8] for global warming over the next decades. The annual inputs of carbon to the life zones are assumed to be as in Table 1 and to continue unchanged. Figure 2 shows that the extra CO_2 carbon evolved in 60 years from soil organic carbon as a result of a rise of 0.02 °C yr^{-1} is 41×10^{15} g; for 0.03 °C yr^{-1}, 61×10^{15} g and for 0.05 °C yr^{-1}, 100×10^{15} g. The corresponding evolution of CO_2 carbon from combustion of fossil fuel over the same 60-yr period will be 320×10^{15} g, if present production[8] (5.4×10^{15} g yr^{-1}) continues unchanged. If warming is confined to northern latitudes, less soil organic carbon will be decomposed than if warming is uniform (Fig. 2). This is because at high latitudes the soil is too cold for appreciable biological activity for much of the year: if the mean monthly temperature for January is −15 °C, an increase of 10 °C will have no effect on decomposition. These calculations suggest that increased decomposition of soil organic carbon will indeed make an important contribution to the greenhouse effect, but that the contribution is unlikely to be a runaway effect, as has been feared[2].

The projections in Fig. 2 are very uncertain: individual predictions could be in error by ±50%. The fits illustrated in Fig. 1 show that the parts of the model which adjust decomposition rates for climate and soil texture are reasonably satisfactory: the model accounts for 83% of the variance in the unselected database. But this base is itself biased by the uneven geographical spread of the experiments, and some life zones are completely unrepresented. Even more serious errors are introduced when the model is fitted to the global data in Table 1: the global stock of soil organic matter itself has a coefficient of variation[9] of ~14%.

The model can also be used to see how changes in precipitation influence decomposition, although on the global scale this must remain an academic exercise until better forecasts of the effect of increasing concentrations of greenhouse gases on precipitation are available. According to the model, in the cool temperate steppe zone, a 25% decrease in precipitation, spread uniformly over the year and starting in 1990, will increase the stock of soil organic carbon from 120×10^{15} g C (see Table 1) to 125×10^{15} g by 2050, the annual input being unchanged throughout. In this zone, lack of moisture retards decomposition during summer, when it would otherwise have been at its fastest. In contrast, neither a 25% increase nor a 25% decrease in rainfall alters the stock of soil organic carbon in the tropical forest wet zone; the soil is always wet enough for decomposition to proceed at its maximum permitted rate.

This work shows how climate change can influence the decomposition process in soil. But the amount of organic carbon present in soil at a particular time is determined both by the rate of decomposition and by the annual input of plant debris, set constant in Table 1 and Fig. 2. To tackle the much larger question of how climate change affects the flux of CO_2 between soil and atmosphere[22–24], our model would have to be coupled to another that specifies how global plant production (and hence annual return of plant debris to soil) is altered by increasing concentrations of greenhouse gases. □

Received 5 December 1990; accepted 11 April 1991.

1. Schleser, G. H. *Z. Naturf.* A**37,** 287–219 (1981).
2. Kohlmaier, G. H., Janacek, A. & Kindermann, J. in *Soils and the Greenhouse Effect* (ed. Bouwman, A. F.) 415–422 (Wiley, Chichester, 1990).
3. Jenkinson, D. S. *Phil. Trans. R. Soc. Lond.* B**329,** 361–368 (1990).
4. Lashof, D. A. *Clim. Change* **14,** 213–242 (1989).
5. Schimel, D. S., Parton, W. J., Kittel, T. G. F., Ojima, D. S. & Cole, C. V. *Clim. Change* **17,** 13–25 (1990).
6. Tinker, P. B. & Ineson, P. in *Soils on a Warmer Earth* (eds Scharpenseel, H. W., Schomaker, M. & Ayoub, A.) 71–87 (Elsevier, Amsterdam, 1990).
7. Franz, E. H. *in Soils on a Warmer Earth* (eds Scharpenseel, H. W., Schomaker, M. & Ayoub, A.) 109–120 (Elsevier, Amsterdam, 1990).
8. *Intergovernmental Panel on Climate Change* (eds Houghton, J. T., Jenkins, G. J. & Ephraums, J. J.) (Cambridge University Press, 1990).
9. Post, W. M., Emanuel, W. R., Zinke, P. J. & Stangenberger, A. G. *Nature* **289,** 156–159 (1982).
10. Jenkinson, D. S., Hart, P. B. S., Rayner, J. H. & Parry, L. C. *INTECOL Bull.* **15,** 1–8 (1987).
11. Jenkinson, D. S. *J. Soil Sci.* **28,** 424–434 (1977).
12. Ayanaba, A. & Jenkinson, D. S. *Soil Sci. Soc. Am. J.* **54,** 112–115 (1990).
13. Oberlander, H. E. *Scr. varia pont. Acad. Sci.* **38,** 1001–1062 (1973).
14. Nyhan, J. W. *Soil Sci. Soc. Am. J.* **39,** 643–648 (1975).
15. Ladd, J. N., Oades, J. M. & Amato, M. *Soil Biol. Biochem.* **13,** 119–126 (1981).
16. Gonzalez, A. M. A. & Sauerbeck, D. R. in *Regional Colloquium on Soil Organic Matter Studies* (eds Cerri, C. C., Athie, D. & Sodrzeieski, D.) 141–146 (CENA/USP & PROMOCET, Piracicaba, 1982).
17. Neue, H. U. & Scharpenseel, H. W. *Sci. Total Envir.* **62,** 431–434 (1987).
18. Voroney, R. P., Paul, E. A. & Anderson, D. W. *Can. J. Soil Sci.* **69,** 63–77 (1989).
19. Holdridge, L. R. *Life Zone Ecology* (Tropical Science Center, San Jose, 1964).
20. Crutzen, P. J. & Andreae, M. O. *Science* **250,** 1669–1678 (1990).
21. Schlesinger, W. H. *Ann. Rev. ecol. Syst.* **8,** 51–81 (1977).
22. Adams, J. W., Faure, H., Faure-Denard, L., McGlade, J. M. & Woodward, F. I. *Nature* **348,** 711–714 (1990).
23. Prentice, K. C. & Fung, I. Y. *Nature* **346,** 48–51 (1990).
24. Schlesinger, W. H. *Nature* **348,** 232–234 (1990).
25. Müller, M. J. *Selected Climatic Data for a Global Set of Standard Stations for Vegetation Science* (Junk, The Hague, 1982).

ACKNOWLEDGEMENTS. We thank D. Barraclough for advice on computer programming, J. I. L. Morison for help in locating climatic data and the Oxford University Computing Serivce for access to computing facilities. This work was supported by the Leverhulme Trust.

Water diffusion in a basaltic melt

Youxue Zhang & E. M. Stolper

Division of Geological and Planetary Sciences, 170-25,
California Institute of Technology, Pasadena, California 91125, USA

WATER is the most abundant volatile component in terrestrial basalts and is a significant constituent of the gases that escape from basaltic magmas. Knowledge of the diffusivity of water (and other volatiles) in basaltic melts is important for understanding the degassing of basaltic magma and for assessing the fractionation of volatiles during degassing. We report here measurements of water diffusivity in a basaltic liquid. The water concentration profiles through the samples, determined by Fourier-transform infrared spectroscopy, cannot be modelled adequately on the basis of a constant water diffusivity[1–7], but instead can be fitted by assuming that only molecular H_2O is diffusing and that there is a local equilibrium between H_2O molecules and OH groups[7–13]. The concentration-dependent total water diffusivities in the basaltic melt at 1,300–1,500 °C are 30–50 times as large as those in rhyolitic melts[4–7], and are greater than the total CO_2 diffusivity in

basaltic melts, contrary to previous expectations[14]. These results suggest that diffusive fractionation would increase the ratio of water to carbon dioxide in growing bubbles relative to equilibrium partitioning, and decrease the ratio in interface melts near an advancing anhydrous phenocryst.

Chips of basaltic glass from the Juan de Fuca (JDF) ridge were used as starting material for this study. The original glass chips contained 0.35–0.43 wt% dissolved total water (hereafter % refers to wt% unless otherwise specified) as measured by FTIR (Fourier transform infrared spectroscopy; see also ref. 15), and some small bubbles (<100 μm) and microphenocrysts (<200 μm), one hundred to several hundred micrometres apart. Water-poor glass was prepared by melting ~10 grams of the JDF basaltic glass powder (contained in a platinum crucible pre-saturated with FeO-bearing basaltic melt) in a 1-atm Deltech furnace at a f_{O_2} corresponding to the quartz–fayalite–magnetite buffer. Glass prepared in this way contains 0.02–0.10% total water (based on FTIR measurement) and is almost free of bubbles and crystals. The partially dehydrated glass is more transparent than the original, more water-rich glass. Even though the water contents of the dehydrated and the original starting glass material are variable, chips the size of those used in experiments (~2 mm in each dimension) are assumed to be uniform (within 5% relative) in water content. This assumption is based on analyses of selected fragments of the glasses.

Each experimental couple consisted of two halves, one a piece of pristine JDF glass and the other a piece of dehydrated JDF glass. Each half was a polished cylindrical disk ~1.5-mm thick and ~2 mm in diameter. The two halves fitted snugly into a graphite capsule, which was enclosed in a platinum capsule and then welded shut. The platinum capsule was placed in a sleeve of crushable MgO and then encased in a 30-mm-long graphite heater. CaF_2 was used as the pressurizing medium. Experiments were conducted in a piston-cylinder apparatus at 1,300–1,500 °C and 1.0 GPa. (An additional experiment was run at 1,250 °C, but the charge partially crystallized.) During the run, the interface between the two halves was roughly horizontal and the water-rich half was above the water-poor half. We used a 'piston-

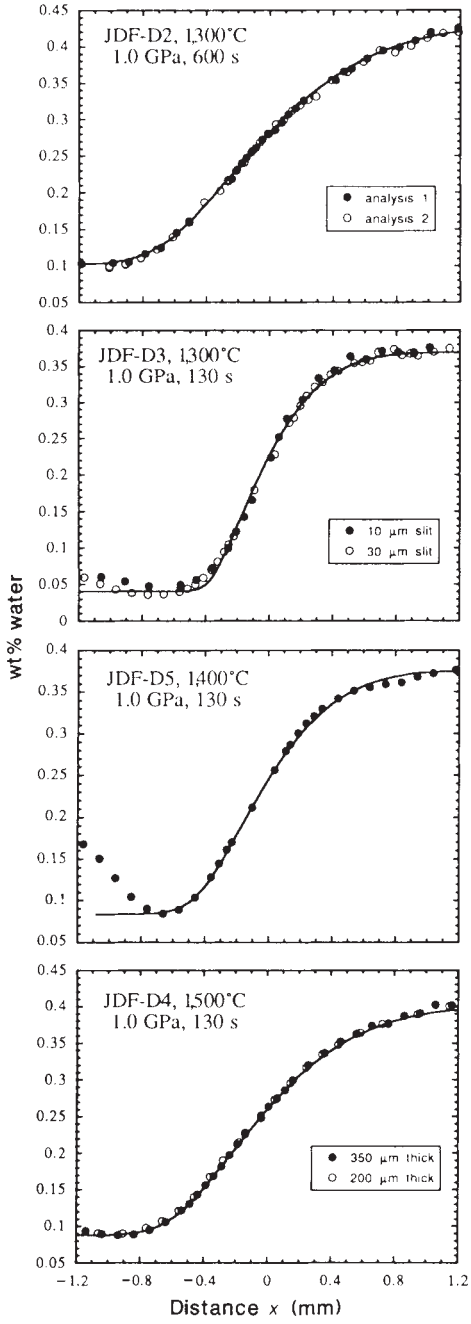

FIG. 1 Total water concentration profiles (points) with run conditions. The curves shown are fits of the data with a water diffusion model in which only molecular H_2O diffuses and there is local equilibrium between H_2O molecules and OH groups. K for all fits was arbitrarily chosen as 0.5. The D_{H_2O} values derived for the four diffusion couples were $(3.23 \pm 0.5) \times 10^{-9}$, $(5.1 \pm 0.2) \times 10^{-9}$, $(7.3 \pm 0.2) \times 10^{-9}$ and $(1.20 \pm 0.02) \times 10^{-8}$ m s^{-2} for JDF-D2, D3, D5 and D4 respectively. The values probably do not correspond to the actual diffusivity of molecular H_2O, as K was estimated by extrapolation from rhyolitic glasses. When K was varied, the quality of the fit changed little, but the best-fit D_{H_2O} values varied roughly proportionately with K (refs 7, 11, 13). D_{H_2O} values for JDF-D2 and JDF-D3 agree within 44%. All fits were done on a molar basis and then recalculated to wt% for plotting. Bulk composition of the basalt (TT152-21) by wt% is: SiO_2, 50.6; TiO_2, 1.88; Al_2O_3, 13.9; FeO_{total}, 12.5; MnO, 0.23; MgO, 6.56; CaO, 11.4; Na_2O, 2.64; K_2O, 0.17; P_2O_5, 0.21 (S. van der Laan, personal communication, and ref. 15). Water concentrations were determined from infrared spectra obtained with a Nicolet 60SX FTIR. A slit (10 μm × 2 mm or 30 μm × 1 mm) was used to delimit the infrared beam. The profiling was done with a translation stage[7]. Total water concentration was determined from the intensity of the absorption band at ~353 mm^{-1} using a molar absorptivity of 63 l mol^{-1} cm^{-1} (ref. 15). Concentrations of individual species, H_2O molecules and OH groups, could not be determined because the water contents were low. Baselines were drawn with a french curve. A small correction (less than 5% relative, depending on the total water concentration) to the peak at ~353 mm^{-1} was sometimes applied for the growth of an ice band in the detector at ~325 mm^{-1} during the measurements. From the quality of the spectra and reproducibility shown in this figure, the 1σ analytical precision in determining total water concentration is ≤2% at ≥0.3% water and ~4% at 0.05% water, less than or equal to the size of the points. The accuracy of the water concentration measurement (which depends on the chosen value of molar absorptivity) does not affect the determination of total water diffusivities. Nor does it affect the model fitting shown here, although it affects actual D_{H_2O} values. The interface shown here is the Matano interface[20] determined from the smoothed concentration profile (actual interface positions were not measured). There are two complications to the concentration profiles. One is the presence of cracks, which can interfere with infrared analyses and complicate distance determinations. Sample JDF-D3 was affected the most by these cracks. The other is a (usually slight) increase in water content towards the end of the water-poor half, possibly due to water in pore spaces in the graphite capsule. The capsule of JDF-D5 was accidentally dropped into water before the platinum capsule was completely sealed. It was subsequently heated in a vacuum furnace at ~110 °C for about half an hour and then welded shut, but is probable that water got into the capsule and was not totally removed. The increase towards the end of the water-poor half was ignored during fitting.

out' procedure (initially overpressurized to ~1.5 GPa) to bring the charge to 1.0 GPa cold, and then heated it. Temperatures were monitored and controlled by a $Pt-Pt_{90}Rh_{10}$ thermocouple connected to an automatic control system. Overshooting and fluctuation in temperature were ≤5 °C and ~1 °C respectively. The temperature difference from the centre to the end of the charge is ~10 °C (ref. 16 and M. B. Baker, personal communication). Experimental durations were 2–10 min. These short run durations were dictated by the high water diffusivities at these temperatures and the short diffusion distance available, and resulted in large relative errors in determining the experiment duration, as the heating took ~0.5 min. To assess this error, a 'zero-time' experiment was carried out at 1,300 °C (the sample was brought up to temperature, then quenched instantly); the concentration profile for this experiment is equivalent to diffusion at 1,300 °C for 8 s. Reported run durations (Fig. 1) are nominal run duration plus 10 s to account for the finite times of heating and quenching.

Each charge was quenched by shutting off the power to the piston-cylinder apparatus. A doubly polished, 200–350-μm-thick slice parallel to the axis of the cylinder was prepared near the widest section of the cylinder. Optical examination showed the charges to be free of crystals and bubbles (except one bubble ~100 μm in diameter in the water-rich side of JDF-D4, probably a residue of a large bubble in the initial glass), suggesting that microphenocrysts and bubbles in the original water-rich glass wafers dissolved into the melt during the experiments. Dissolution of bubbles and microphenocrysts had little effect on the water concentration profile, but it had a significant effect on the carbonate concentration profile (discussed later) because the dissolution doubled the CO_2 content of the glass. The degree of transparency varied across the charge, the water-rich side being less transparent as in the original glass chips.

Figure 1 shows the experimental conditions, analytical procedures and resulting total water concentration profiles. The diffusion medium is assumed to be infinite. If the profiles could be characterized by a constant total water diffusivity, they would be symmetric about the interface and fitted well by error functions, but Fig. 1 shows that the concentration profiles are not symmetric. When the profiles are fitted to an error function, there are systematic discrepancies between the data and the fit, except for JDF-D3. The inability of a constant $\overline{D^*_{water}}$ (average total water diffusivity[7]) to account in detail for water diffusion profiles in silicate melts and glasses is well known[1–7]. The $\overline{D^*_{water}}$ values thus obtained (2.5×10^{-10}, 2.9×10^{-10}, 4.7×10^{-10} and 8.4×10^{-10} $m^2\ s^{-1}$ for JDF-D2, JDF-D3, JDF-D5 and JDF-D4), although imperfectly fitting the concentration profiles, characterize the mean transport rate of water under these conditions. The two experiments at 1,300 °C (JDF-D2 and JDF-D3), had run durations that differed by a factor of 5, but their $\overline{D^*_{water}}$ values agree to within 20% (formal 1σ errors for $\overline{D^*_{water}}$ values of both samples based on fits of profiles are ~5%), demonstrating diffusion control of the experiments and providing an estimate of uncertainties in $\overline{D^*_{water}}$.

We also tested the data against a model in which only H_2O molecules diffuse[7–13], although the dominant hydrous species at these low water contents is expected to be OH. Local equilibrium was assumed[17], with an equilibrium constant $K = 0.5$ chosen for the reaction

$$H_2O + O_{dry} = 2\ OH \qquad (1)$$

where O_{dry} refers to anhydrous oxygen[18]. The water concentration profiles were fitted following the procedure of Zhang *et al.*[7] and the resulting fits are given in Fig. 1. In general, good fits are obtained, suggesting that molecular H_2O is the diffusing species for water diffusion in the basaltic melt, as found previously for silica[8,12] and rhyolitic glasses[7].

The variation of D^*_{water} (apparent total water diffusivity[7]) with total water content was calculated for each experiment from the best fit values of D_{H_2O} (diffusivity of molecular H_2O) for a given value of K by using the following expression[7,19]

$$D^*_{water} = D_{H_2O}\,d[H_2O]/d[water], \qquad (2)$$

where quantities in brackets represent mole fractions and $[water] = [H_2O] + 0.5[OH]$ (ref. 18). Calculated values of D^*_{water} are shown as a function of water content in Fig. 2*a*. The values of D^*_{water} are almost proportional to total water content at these low water contents[7,8,11]. We have also calculated D^*_{water} values using a Boltzmann–Matano analysis[20] of the concentration profiles, and these D^*_{water} values are compared with those calculated from (2) in Fig. 2*a*. They are in reasonable agreement, but D^*_{water} values obtained using the Boltzmann–Matano analysis show more scatter because errors arise from uncertainties in evaluating numerical derivatives and integrals.

The partially dehydrated starting glass chips were also partially decarbonated, and there is therefore a carbonate profile between the two halves of the diffusion couple. The graphite capsule also provides a source of carbonate to the basaltic melt (from oxidation of graphite by ferric iron) which diffuses inward into the melt. These carbonate concentration profiles were determined with the FTIR for JDF-D2. We only consider the profile adjacent to the graphite capsule in the initially decarbonated half because other profiles were affected considerably by dissol-

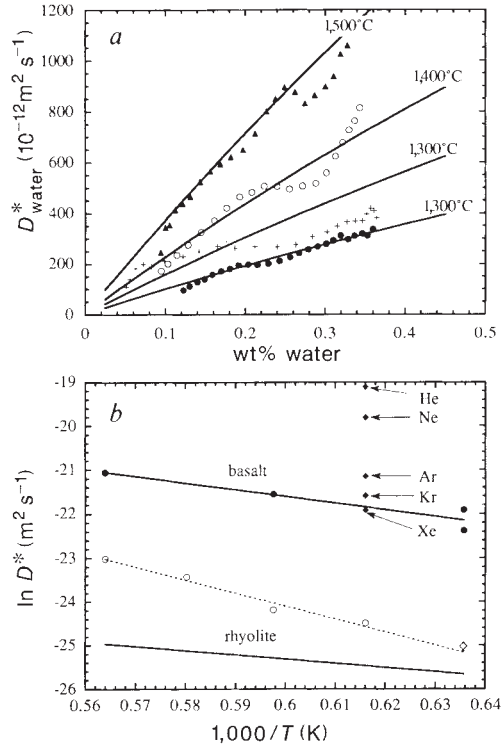

FIG. 2 *a*, Comparison of D^*_{water} values obtained from Boltzmann–Matano analysis (points) with those calculated from equation (2) based on the fits in Fig. 1 (solid lines). ●, 1,300 °C (JDF-D2); +, 1,300 °C (JDF-D3); ○, 1,400 °C (JDF-D5); ◆, 1,500 °C (JDF-D4). Note that at our water concentration levels, D^*_{water} values calculated from equation (2) are almost independent of the choice of K because the dependences of D_{H_2O} and $d[H_2O]/d[water]$ on K cancel: that is, at these low water contents, D_{H_2O} is almost proportional to K, and $d[H_2O]/d[water]$ is almost inversely proportional to K (at very low water content[7], $d[H_2O]/d[water] = 8[water]/K$). *b*, Apparent total water diffusivities at 0.2 wt% total water in a natural basaltic melt at 1.0 GPa (filled circles and upper solid line, this study) and in rhyolitic melt at 0.1 or 70 MPa extrapolated from lower temperature data[4,7] (lower solid line). Nominal 1σ errors for diffusivities from this study are roughly the size of the symbol. Also shown are apparent carbonate diffusivities in an iron-free synthetic 'basaltic' melt at 1.5 GPa (○ and – – –)[14] and in the JDF basalt at 1,300 °C and 1.0 GPa (◇, this study), and noble gas diffusivities in a tholeiitic basaltic melt at 1,350 °C and 0.1 MPa (◆)[32].

ution of bubbles. The profile can be fitted well if we assume a constant CO_3^{2-} concentration at the graphite–melt interface for the duration of the experiment and constant apparent carbonate diffusivity[13] of $(13 \pm 1) \times 10^{-12}$ m^2 s^{-1} (nominal 1σ error). This diffusivity agrees well with the value ($\sim 11 \times 10^{-12}$ m^2 s^{-1}) extrapolated from data[14] for an iron-free model 'basaltic' melt at 1.5 GPa. Note that there must be a f_{O_2} profile accompanying the carbonate profile adjacent to the graphite[21] in each of our experiments, and that determinations of carbonate concentrations in melts enclosed in graphite capsules can be used to measure f_{O_2}.

Diffusivity values at 0.2% water in basaltic melts calculated from equation (2) can be fitted by the following Arrhenius relation:

$$\ln D^*_{water}\,(m^2\,s^{-1}) = -(12.49 \pm 2.35) - (15200 \pm 3900)/T(K) \quad (3)$$

At other low water contents D^*_{water} can be estimated from the total water content, to which it is roughly proportional. Figure 2*b* compares diffusivities of various components. The activation energy for total water diffusion at 0.2% total water in the basaltic melt is 126 ± 32 kJ mol^{-1}, slightly higher than that in rhyolitic melt ($\sim(103-23) = \sim 80$ kJ mol^{-1}; see refs 4, 7 for details), but significantly lower than that for apparent carbonate diffusion in iron-free 'basaltic' melt (249 ± 30 kJ mol^{-1}; see ref. 14). Values of D^*_{water} at 0.2% water in the basaltic melt are 30–50 times those in rhyolitic melts and 7–10 times the apparent carbonate diffusivities in the JDF basalt or the iron-free 'basalt'. For the D^*_{water} values to be identical to the apparent carbonate diffusivity at 1,300 °C would require total water content as low as 0.02%, lower than the water contents of typical natural basaltic melts[15,22–26]. Diffusivities of noble gas elements are in general higher than the apparent diffusivity of carbonate but may overlap with the total water diffusivity, depending on the water content.

These water diffusion data can be used to evaluate diffusive fractionation between different volatile components during bubble and crystal growth in basaltic melts. Watson *et al.*[14] discussed such fractionations between carbon dioxide and water, but assumed that water diffusivities extrapolated from data in rhyolitic melt could be applied to basaltic melts; in other words, that the apparent diffusivity of total water in basaltic melts is lower than that of carbonate. Our data show that the opposite is true, and their conclusions must be reversed. For example, diffusive fractionation would increase the ratio of water to carbon dioxide in bubbles grown from oversaturated melt above that expected from equilibrium partitioning, but decrease the ratio in interface melts adjacent to advancing anhydrous phenocrysts.

Bubbles in mid-ocean-ridge basalts have varied ratios of H_2O/CO_2 and varied fractions of minor and trace components such as N_2, H_2, CO, SO_2 and noble gases[27–29]. Part of these variations may be due to the diffusive control on bubble composition. Because mid-ocean-ridge basalts are often oversaturated with respect to CO_2-rich vapour when they are erupted on the sea floor[15,30] (that is, bubbles do not reach equilibrium with the bulk melt during rapid ascent), the diffusive transport of volatiles must play some part in controlling bubble growth rates and bubble composition. In addition, the compositions of multicomponent gas bubbles (for example, the H_2O/CO_2, He/CO_2 ratios and noble gas patterns) in the transient bubble growth stage depend strongly on the solubilities and diffusivities of the various volatile components[31]. If equilibrium is not reached for any volatile component, each component would interact only by diffusive transport with the adjacent melt that is on average $\sim 2\sqrt{D_i t}$ away from the bubble, where D_i is diffusivity for component *i*. In this extreme case, bubbles could have a He/Xe ratio higher than expected from equilibrium partitioning. It is more likely that equilibrium can be reached for rapidly diffusing components such as He but not for slowly diffusing components such as CO_2. Kinetic fractionations of this sort may be important in the evolution of bubble compositions and compositional differences between smaller and larger bubbles. With our new data on water diffusivity in basaltic melts and previous data on carbonate and noble gas diffusivities[14,32,33], it should be possible to model in detail the evolution of bubble composition as a function of depth during magma ascent. It may also be possible to infer magma ascent rates from the diffusion profiles of volatile components adjacent to bubbles. □

Received 27 December 1990; accepted 10 April 1991.

1. Roberts, G. J. & Roberts, J. P. *Phys. Chem. Glass.* **5,** 26–32 (1964).
2. Burn, I. & Roberts, J. P. *Phys. Chem. Glass.* **11,** 106–114 (1970).
3. Delaney, J. R. & Karsten, J. L. *Earth planet. Sci. Lett.* **52,** 191–202 (1981).
4. Karsten, J. L., Holloway, J. R. & Delaney, J. R. *Earth planet. Sci. Lett.* **59,** 420–428 (1982).
5. Lapham, K. E., Holloway, J. R. & Delaney, J. R. *J. non-cryst. Solids* **67,** 179–191 (1984).
6. Stanton, T. R., Holloway, J. R., Hervig, R. L. & Stolper, E. M. *Eos* **66,** 1131 (1985).
7. Zhang, Y., Stolper, E. M. & Wasserburg, G. J. *Geochim. cosmochim. Acta* **55,** 441–456 (1991).
8. Doremus, R. H. in *Reactivity of Solids, Proc. 6th Int. Symp.* (ed. Mitchell, J. W.) 667–673 (Wiley Interscience, 1969).
9. Ernsberger, F. M. *Phys. Chem. Glass.* **21,** 146–149 (1980).
10. Smets, B. M. & Lommen, T. P. *Phys. Chem. Glass.* **24,** 635–36 (1983).
11. Wasserberg, G. J. *J. Geol.* **65,** 15–23 (1988).
12. Wakabayashi, H. & Tomozawa, M. *J. Am. Ceram. Soc.* **72,** 1850–1855 (1989).
13. Zhang, Y., Stolper, E. M. & Wasserburg, G. J. *Earth planet. Sci. Lett.* (in the press).
14. Watson, E. B., Sneeringer, M. A. & Ross, A. *Earth planet. Sci. Lett.* **61,** 346–358 (1982).
15. Dixon, J. E., Stolper, E. M. & Delaney, J. R. *Earth planet. Sci. Lett.* **90,** 87–104 (1988).
16. Zhang, Y., Walker, D. & Lesher, C. E. *Contr. Miner. Petrol.* **102,** 492–513 (1989).
17. Zhang, Y., Stolper, E. M. & Ihinger, P. D. *V. M. Goldschmidt Conf. Abstr.* 94 (1990).
18. Stolper, E. M. *Contr. Miner. Petrol.* **81,** 1–17 (1982).
19. Chekhmir, A. S., Epel'Baum, M. B. & Simakin, A. G. *Geohkimiya* **10,** 303–305 (1988).
20. Crank, J. *The Mathematics of Diffusion* (Oxford University Press, Oxford, 1975).
21. Dunn, T. *Geochim. cosmochim. Acta* **47,** 1923–1936 (1983).
22. Delaney, J. R., Muenow, D. W. & Graham, D. G. *Geochim. cosmochim. Acta* **42,** 581–594 (1978).
23. Muenow, D. W., Graham, D. G. & Liu, N. W. K. *Earth planet. Sci. Lett.* **42,** 71–76 (1979).
24. Harris, D. M. *J. Geol.* **89,** 689–701 (1981).
25. Harris, D. M. & Anderson, A. T. Jr, *Geochim. cosmochim. Acta* **47,** 1139–1150 (1983).
26. Kyser, T. K. & O'Neil, J. R. *Geochim. cosmochim. Acta* **48,** 2123–2133 (1984).
27. Moore, J. G., Batchelder, J. N. & Cunningham, C. G. *J. Volcan. geotherm. Res.* **2,** 309–327 (1977).
28. Pineau, F. & Javoy, M. *Earth planet. Sci. Lett.* **62,** 239–257 (1983).
29. Jambon, A. & Zimmermann, J. L. *Chem. Geol.* **62,** 177–189 (1987).
30. Stolper, E. M. & Holloway, J. R. *Earth planet. Sci. Lett.* **87,** 397–924 (1988).
31. Cable, M. & Frade, J. R. *J. Mater. Sci.* **22,** 919–924 (1987).
32. Lux, G. *Geochim. cosmochim. Acta* **51,** 1549–1560 (1987).
33. Carroll, M. R. *Eos* **71,** 1664 (1990).

ACKNOWLEDGEMENTS. We thank M. R. Carroll for comments and S. van der Laan for providing the JDF glasses; Y.Z. thanks M. B. Baker for technical assistance. This work is supported by NSF and NASA.

High-temperature electrical conductivity of the lower-mantle phase (Mg, Fe)O

B. J. Wood & J. Nell

Department of Geology, Bristol University, Wills Memorial Building, Queens Road, Bristol BS8 1RJ, UK

THE electrical conductivity of the lower mantle, which controls the transmission of geomagnetic signals to the Earth's surface, has been the subject of recent controversy[1,2]. Peyronneau and Poirier[1] extrapolated high-pressure conductivity measurements of the lower-mantle assemblage (Mg, Fe)SiO_3 perovskite plus (Mg, Fe)O magnesiowüstite from 673 K to lower-mantle temperatures (2,200–2,500 K) to obtain conductivities consistent with geomagnetic observations (~ 1 S m^{-1} at 1,000-km depth). The high-pressure study of Li and Jeanloz[2] gave conductivities several orders of magnitude lower. Here we report measurements of conductivity and thermopower of the iron-rich phase (Mg, Fe)O at high temperature (1,173–1,773 K) and controlled oxygen partial pressure (pO_2). We find that pO_2 has a very large influence on conductivity: at fixed temperature and pressure, changes in pO_2 can vary the conductivity by 1.5 orders of magnitude within the stability field of magnesiowüstite. For plausible mantle values of pO_2, temperature and bulk composition, we obtain results in good agreement with those of ref. 1, indicating that magnesiowüstite is the dominant conductor in the lower mantle and that observed upper- and lower-